PCCP

PAPER

View Article Online
View Journal | View Issue

Cite this: *Phys. Chem. Chem. Phys.*, 2018, **20**, 29804

Room temperature d^0 ferromagnetism in PbS films: nonuniform distribution of Pb vacancies

Artem Pimachev, Gaurab Rimal, Robert D. Nielsen, Jinke Tang and Yuri Dahnovsky *

Received 31st July 2018,
Accepted 9th November 2018

DOI: 10.1039/c8cp04882g

rsc.li/pccp

Because of the importance of ferromagnetism at room temperature, we search for new materials that can exhibit a non-vanishing magnetic moment at room temperature and at the same time can be used in spintronics. The experimental results indicate that d^0 ferromagnetism without any magnetic impurities takes place in PbS films made of close-packed lead sulfide nanoparticles of 30 nm. To explain the existence of the d^0 ferromagnetism, we propose a model where various PbS bulk and surface configurations of Pb-vacancies are analyzed. The bulk configurations have a zero magnetic moment while the two surface configurations with Pb vacancies with the same non-vanishing magnetic moments and lowest ground state energies contribute to the total magnetization. Based on the experimental value of the saturation magnetization, 0.2 emu g^{-1}, we have found that the calculated Pb vacancy concentration should be about 3.5%, which is close to typical experimental values. Besides being very important for applications, there is one feature of PbS d^0 ferromagnetism that makes this material special for fundamental research: PbS ferromagnetism can exhibit topologically driven spatial magnetic moment distributions (*e.g.*, magnetic skyrmions) due to large spin–orbit coupling.

I. Introduction

Diluted magnetic semiconductors (DMSs) have been intensively studied in the last few decades to reduce or decrease the gap between spintronics and traditional electronics.[1,2] Much research has been done on II–VI and III–V DMSs, especially semiconductors doped by transition metal (TM) impurities where many unusual magnetic and optical properties have been observed in their nanocrystals.[3–21] Because of the importance of ferromagnetism at room temperature for various applications in DMSs, much research has been focused on investigating DMS materials that satisfy this criterion. Different types of dopants can substantially change the value of a magnetic moment in metal-oxide nanocrystals. For example, in In_2O_3 quantum dots (QDs) doped with Cr^{3+} impurities, ferromagnetism is sensitive to the QD crystal structure. Indeed, for bcc-In_2O_3 nanocrystals, the saturation magnetic moment is much greater than that of rh-In_2O_3 quantum dots.[22] As shown in ref. 23, different types of TM impurities can enhance or suppress the ferromagnetism in In_2O_3 or SnO_2 quantum dots. Fe^{3+} decreases the magnetization while Mn^{2+} significantly enhances the ferromagnetism. In addition, oxygen vacancies are able to influence the electron transport properties. In In_2O_3 nanocrystals, the 2D electron mobility can be increased because of the metal–insulator transition due to the presence of O-vacancies.[24] It was theoretically predicted that room temperature ferromagnetism exists in Mn doped GaN[25] and then it was experimentally confirmed in ref. 26–28. There is another type of ferromagnetic material with a T_c much above room temperature and with no TM doping.[29–36] Such nanocrystals exhibit d^0 (d or f electrons are not involved) ferromagnetism associated with unpaired electron spins due to the intrinsic defects – vacancies. ZnO and ZnS are such nanocrystals that demonstrate d^0 ferromagnetism.[37–41]

It was found that a ZnS nanocrystal with Zn vacancies also exhibits d^0 ferromagnetism. Theoretical calculations predicted a much higher magnetization than the experimental value.[37] Such a discrepancy was discussed in ref. 38. It was found that the dramatic decrease in magnetization is likely due to the condensation of Zn vacancies into a droplet (or droplets). Thus, the total magnetization essentially depends on the vacancy arrangement or configuration.

There is another interesting magnetic semiconductor, zinc oxide.[30,33,42–54] ZnO nanocrystals have been intensively studied, and the behavior of d^0 ferromagnetism was found to vary. Zhigang Li *et al.*[39] discovered the dramatic dependence of magnetic moment on NC size. Indeed, the magnetization drops by 2–3 orders of magnitude with nanocrystal size. Moreover, the samples become very sensitive to an oxygen-rich environment that reduces the magnetization by approximately five times compared to a similar experiment in a vacuum. The explanation of the drop in magnetization by 2.5 orders of magnitude is

Department of Physics & Astronomy/3905, 1000 E. University Avenue, University of Wyoming, Laramie, WY 82071, USA. E-mail: yurid@uwyo.edu

provided in ref. 40. It was found that some vacancy configurations can have large or very small (zero) magnetic moments. Thus, the vacancy distribution is extremely crucial for the creation of non-vanishing magnetization. Another important feature is where the vacancies are located, *i.e.*, in the bulk or on the surface of a nanocrystal. It was found that the main contribution of Zn vacancies is on the surface.[40] In ref. 41, how to identify bulk or surface vacancy locations from optical spectra is described.[41]

In this research, we continue the quest for new d^0-ferromagnetic materials. The material of our study is lead sulfide. We pay much attention to lead sulfide because PbS is one of the most important narrow gap semiconductors used for infrared detectors. There is another fundamental feature of PbS – this material has large spin–orbit coupling (SOC). The large spin–orbit coupling can lead to unusual magnetic behaviors. In particular, magnetic topological structures, *e.g.*, skyrmions, are possible in PbS crystals. As the first step of this research, we experimentally observe ferromagnetism in a film made of closely packed nanoparticles of 30 nm. To explain the origin of the PbS ferromagnetism, we introduce a model capable of describing and understanding the experimental data. In ref. 21, the authors found ferromagnetism at a high transition temperature in both undoped and Mn doped PbS nanowires. Carrier–dopant exchange interactions in Mn-doped PbS quantum dots and crystals were studied by using polarized light.[55,56]

In this work, we present the experimental proof of the existence of room temperature ferromagnetism in PbS films with Pb vacancies and provide the theoretical/computational explanation of the origin of this phenomenon. We prove that the origin of the observed ferromagnetism is the presence of Pb vacancies on the film surface. We also conclude that the Pb vacancies have to be arranged in special configurations rather than uniformly distributed over the whole PbS film.[57]

II. Experimental results

PbS films with a thickness of about 300 nm were deposited on Si substrates using pulsed laser deposition (PLD). The PLD target was prepared by combining appropriate proportions of lead acetate (99.999%, Sigma Aldrich) and sodium sulfide (99.99%, Sigma Aldrich) in aqueous solution, and the precipitates were thoroughly cleaned and dried. X-ray diffraction showed that the resulting powders are in the PbS rock-salt phase. The powders were ground and cold-pressed to prepare a target for PLD. The details of the film preparation can be found in ref. 58 and 59. We undertook extensive XRD analyses of the samples. The standard PbS peaks, along with an extra peak from Pb (the peaks at 31.5° and 36° (marked with asterisks)), are shown in Fig. 1. After annealing, the lattice constant decreases from 5.92 Å to 5.89 Å, as shown in Fig. 1 by the peak shift to a higher 2θ angle. This shift is likely due to the creation of vacancies during annealing. Note that the sample was cut after the preparation and the latter piece was used for annealing. The decrease in intensity of the XRD data is due to the use of a smaller slit during measurements. The overall grain size remains approximately similar after annealing, as shown by the similar peak width in Fig. 1.

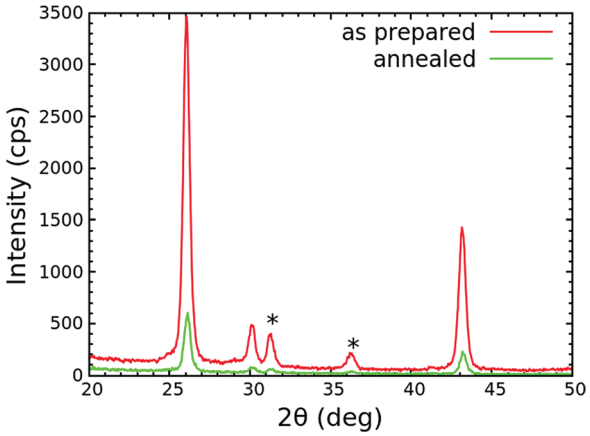

Fig. 1 X-ray diffraction patterns of the as-prepared and annealed samples.

The films were also characterized using scanning electron microscopy (SEM) and atomic force microscopy (AFM). The average particle size of PbS was found to be about 30 nm, as determined from AFM measurements. The XRD results confirmed the rock-salt phase of the films, although there is an impurity phase of Pb metal present in the samples, which is inherent to the preparation method. The presence of these Pb clusters has an important consequence in Pb vacancy formation, and therefore, in the magnetic properties of the films of close-packed nanoparticles of 30 nm. Heating in a high vacuum environment helps to create vacancies, therefore we carried out annealing experiments to test the effects on the vacancies. Annealing was performed in the same vacuum chamber after the initial deposition. The sample was cut and then mounted into the chamber where it was heated to 400 °C and annealed at a pressure of ~10 μTorr for 12 h. The magnetic measurements were done using a Quantum Design's PPMS system.

Fig. 2(a) and (b) show the magnetic hysteresis loops of the as-deposited film and the annealed film measured at room temperature. As can be seen in Fig. 2, the annealed samples are ferromagnetic at room temperature with the coercivity $H_c \sim 35$ Öe. The saturation magnetization of the as-prepared sample is about 2×10^{-2} emu g^{-1}, and that of the annealed sample is 2×10^{-1} emu g^{-1}. When the as-prepared film is annealed in a vacuum, the saturation magnetization increases.

It was anticipated that during annealing, the high vapor pressure of sulfur leads to its removal, thus creating sulfur vacancies. This seems to contradict our understanding of Pb vacancy-induced ferromagnetism. To address this issue, we performed energy calculations on the migration of Pb atoms as a result of the presence of S vacancies, as shown in Fig. 3.

The calculations found that Pb atoms located in the vicinity of a Pb metal cluster have the tendency to migrate to the Pb layer, creating Pb vacancies in the PbS crystal. We computationally found that this physical picture is energetically favorable. Indeed, the energy for the state where Pb atoms from the

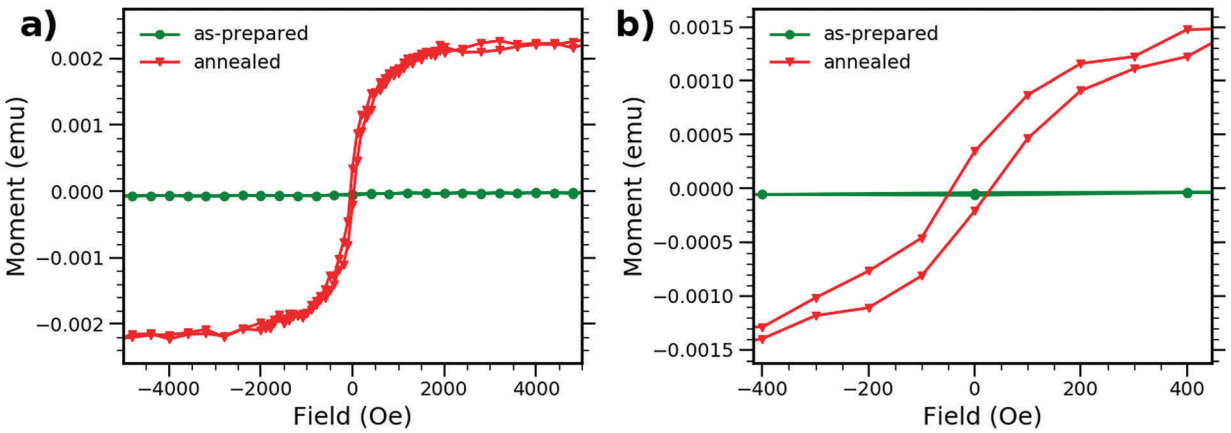

Fig. 2 (a) Magnetic hysteresis of the as-prepared and annealed PbS at room temperature. (b) Magnified view of the hysteresis shown in (a).

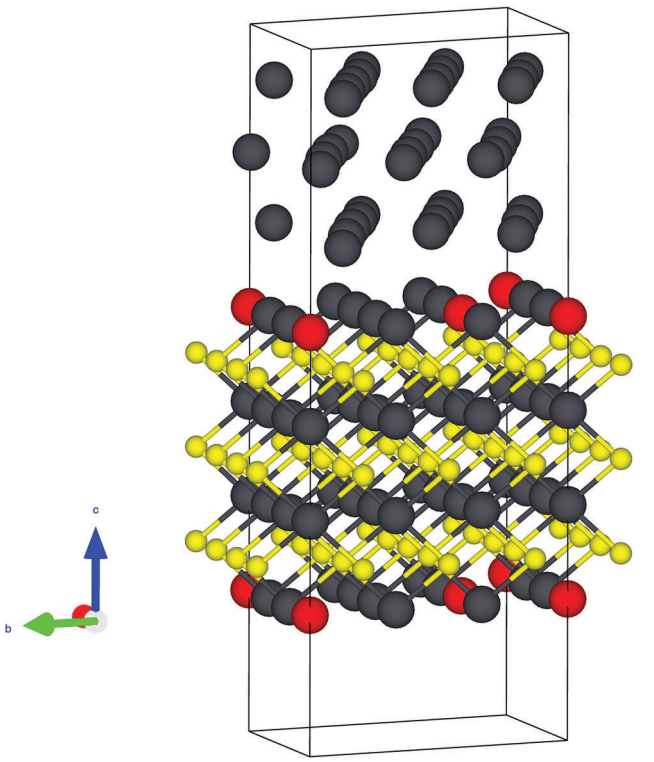

Fig. 3 Pb metal layers on the surface of PbS crystals with vacancies underneath. Pb atoms are in gray, sulfur atoms are in yellow, and lead vacancies are in red.

PbS crystal migrate to the Pb cluster surface (see Fig. 3) is lower by 1.85 eV per Pb-atom compared to when the Pb atoms stay in the PbS crystal. Upon annealing, this creates an additional local magnetic moment, leading to the enhancement of the saturation magnetization.

III. Computational details

To explain the experimental data, we propose a model that consists of both bulk and surface Pb vacancy configurations, each with unique Pb vacancy groups. The first principles calculations were performed using the Vienna Ab Initio Simulation Package (VASP)[60–64] and ELK FP-LAPW codes.[62,64–67] For the VASP calculations, we employ the General Gradient Algorithm (GGA) with the PBE exchange–correlation functional[68–72] that includes spin polarization and tetrahedron smearing.[73] For the PAW pseudo-potentials,[60,61,74] an energy cutoff of 400 eV is employed. The geometries of all vacancy configurations were optimized within VASP to an accuracy of 0.1 meV. To find the spatial magnetization density distribution, we used the ELK FP-LAPW codes.[65] The magnetization vector field over a supercell for a bulk PbS crystal, in which the Pb vacancies induce a high magnetic moment, was investigated within the latter code. For these calculations, the muffin-tin radii of Pb and S were chosen as 1.42 Å and 1.12 Å, respectively. We also included spin–orbit coupling (SOC) in the second-variational procedure[75,76] to an accuracy of 10 meV. The muffin-tin wavefunctions with an angular momentum of up to $L = 14\ \hbar$ were included. For a higher accuracy in the magnetization calculations, we included ten additional unoccupied states, as recommended in ref. 65.

IV. Results and discussion

The main goal of the theoretical investigation was to explain the experimentally observed room temperature d^0 ferromagnetism in PbS films. We checked many Pb-vacancy configurations with one, two, three, four, and five Pb vacancies in the extended unit cell ($3 \times 3 \times 3$) in the bulk and on the surface of the film and found that the one, two, three, and four Pb-vacancy configurations exhibit antiferromagnetism with a zero magnetic moment. Therefore, they should be disregarded as contradictive to the experimental data. Only five Pb-vacancy configurations exhibit ferromagnetism, explaining the experimental data. We then found their ground-state energies and compared them with each other. The configuration with the lowest ground state energy should be selected as the appropriate configuration to explain the experimental data. If it happens that a configuration with the lowest ground state energy has a zero magnetic moment, this configuration should be disregarded

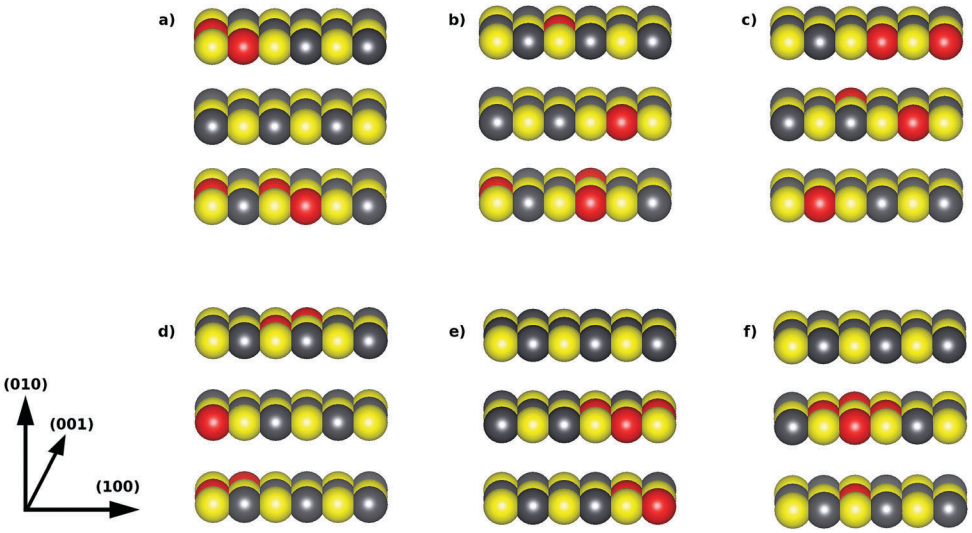

Fig. 4 Bulk Pb-vacancy configurations in a PbS crystal. Pb atoms are shown in gray with sulfur atoms shown in yellow and Pb-vacancy locations for each configuration are shown in red.

because it cannot explain the experimental non-zero value of the magnetization.

First, we studied the bulk configurations. The schematic pictures of these configurations are presented in Fig. 4.

The ground-state energies and magnetic moments calculated in VASP are presented in Table 1 for the selected five Pb-vacancy bulk configurations.

In Table 1, the only configuration with a non-vanishing magnetic moment is the configuration of Bulk F. This configuration is shown in Fig. 5 in more detail, matching a similar picture presented in Fig. 4(f). However, the configuration with the lowest ground state energy is different. It is the configuration of Bulk D. The energy difference between configurations of Bulk D and Bulk F is 1 eV. Taking into account that the bulk vacancy configurations contain five vacancies, we found the energy per vacancy, ΔE. The energy per vacancy difference between the above-mentioned Pb-vacancy configurations is 0.2 eV. Such a difference is greater than k_BT, and therefore, the Bulk D configuration with zero magnetization is more favorable. Thus, the bulk vacancy configurations are not able to explain the experiment.

The energy, ΔE, and the relative energy differences per vacancy are defined as the difference between the total energy of a supercell with vacancies and the total energy of a supercell without vacancies. For the relative energy difference per vacancy, we divide the energy differences by the number of vacancies, N_{vac}, in a supercell. As mentioned above, there are five vacancies

Table 1 Energy and magnetic moment results of the DFT calculations for the bulk configurations shown in Fig. 4

	Bulk A	Bulk B	Bulk C	Bulk D	Bulk E	Bulk F
Energy, eV	−206.37	−206.60	−206.33	−206.87	−206.34	−205.88
Moment, μ_B	0.00	0.00	0.00	0.00	0.00	0.83
ΔE, eV	0.50	0.27	0.54	0.00	0.53	0.99
ΔE_{Full}/Vac, eV	6.08	6.03	6.09	5.98	6.08	6.18

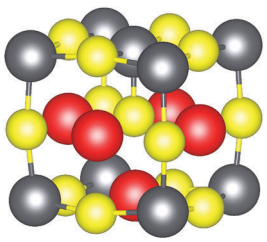

Fig. 5 Bulk vacancy configuration of Bulk F that provides a non-vanishing magnetic moment.

in the bulk and four vacancies in the surface configurations. The relative energy difference $\Delta E_{full}/N_{vac}$ is defined using the following equation:

$$\frac{\Delta E_{full}}{N_{vac}} = \frac{E_{full} - E_{config}}{N_{vac}}. \quad (1)$$

Since the bulk configuration with the lowest energy was antiferromagnetic, the next step was to study the surface Pb-vacancy configurations shown in Fig. 6.

We calculated four different surface configurations with Pb and S surface terminations, as presented in Fig. 6 and 7. For all vacancy configurations, we calculated the magnetic moments and ground state energies. The results are given in Table 2. Both configurations, Surface A and Surface B, shown in Fig. 8, provide a non-vanishing magnetization with the lowest ground state energy.

In this table, Surface A and B vacancy configurations represent the Pb-surface terminations while Surface C and D vacancy configurations denote the S-surface terminations, as shown in Fig. 6. From Table 2, we can see now that there are several vacancy configurations that have non-vanishing magnetizations. They are the configurations of Surfaces A, B, and C. Then, we verified their ground state energies. We found that the configurations of Surfaces A and B have the lowest ground state

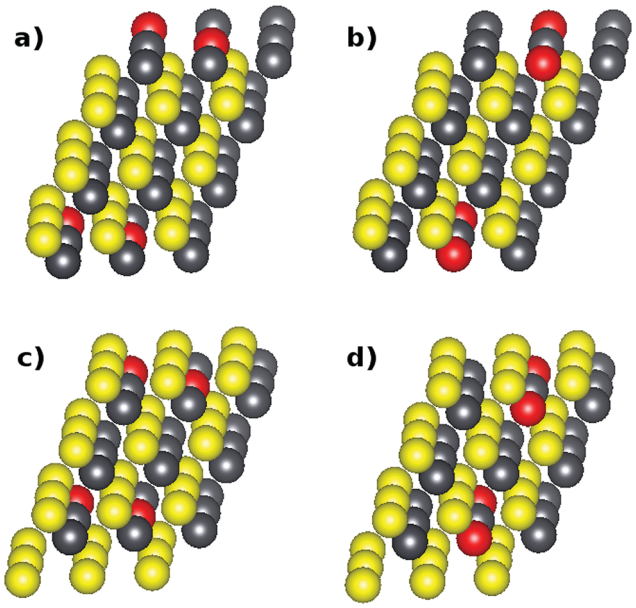

Fig. 6 Surface Pb-vacancy configurations. Pb atoms are shown in gray with sulfur atoms shown in yellow and Pb-vacancy locations for each configuration are shown in red. (a) and (b) are Pb terminated and (c) and (d) are S terminated.

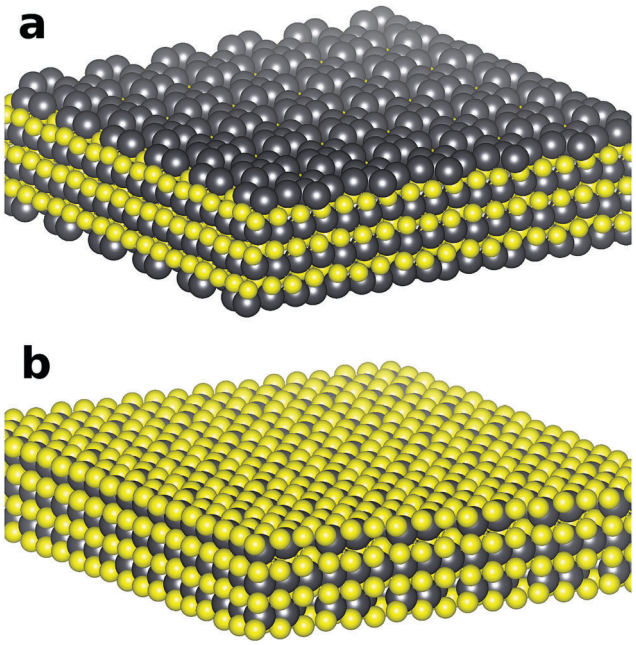

Fig. 7 Surface layers with (a) Pb and (b) S surface terminations, respectively.

energies. These configurations have almost the same magnetic moment per vacancy and both contribute to the total film magnetization.

Having identified the most probable surface vacancy configurations, we compared their ground state energies with the bulk configuration energies. Because the bulk and surface unit cells contain different numbers of vacancies, five for the bulk and four for the surface, we calculated the energy per vacancy,

Table 2 Energy and magnetic moment results of DFT calculations for the surface configurations shown in Fig. 6

	Surface A	Surface B	Surface C	Surface D
Energy, eV	−246.49	−246.49	−235.11	−236.19
Moment, μ_B	1.40	1.40	0.92	0.00
ΔE, eV	0.00	0.00	11.38	10.30
ΔE_{Full}/Vac, eV	2.87	2.87	6.74	6.47

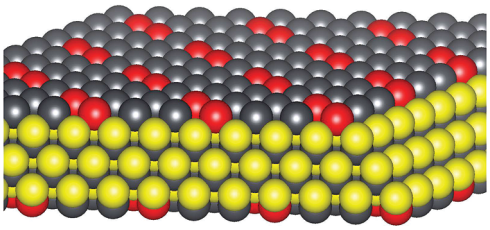

Fig. 8 Surface Pb vacancy configuration of Surface A with the vacancies shown in red.

as described using eqn (1). From the comparison of ground-state energies for the configurations of Bulk D and Surfaces A and B, we conclude that the surface configurations are much more favorable with a ground-state energy difference of about 3.3 eV.

In the experiments, the film is made of close-packed nanoparticles of about 30 nm in size. Considering a spherical nanoparticle, we estimated the concentration of vacancies to fit the experimental value of magnetization per volume. Based on the experimentally measured saturation magnetization, the PbS slab size, and the magnetic moment per surface vacancy (see Table 2), we found that the estimated concentration of Pb vacancies is about 3.5%, which is close to a typical experimental value.[77]

In the experiment, there was the observation of Pb-metal islands. This picture is confirmed by the calculations that are in favor of Pb rather than S surface terminations.

We also verified the magnetization value in the presence of S-vacancies. We found that the magnetic moment vanishes in this case.

V. Conclusions

As was believed before,[57] the magnetic moment in a PbS nanocrystal is zero, indicating the antiferromagnetic arrangement. However, a non-zero value of magnetization was observed in experiments, where the magnetization dependence on an applied magnetic field is shown in Fig. 2(a) and (b). To explain the experimental data, we have proposed a model where some special configurations of Pb-vacancies can exhibit non-vanishing magnetic moments. In this model, we considered six bulk Pb vacancy configurations (see Fig. 4 and also Table 1) and found that the configuration with the lowest ground state energy is configuration Bulk D. However, this configuration has a zero magnetic moment and cannot explain the experimental non-zero magnetization value. We then studied surface configurations (see Fig. 6) in two different cases with Pb and S terminations

(see Fig. 7). We found that the two configurations Surfaces A and B shown in Fig. 6 have the lowest ground state energies with non-zero magnetic moments (see Table 2). It is interesting to note that the contribution of these configurations is equal; however, they are two very different configurations. Based on the experimental value of magnetization, 0.2 emu g^{-1}, we estimated the concentration of vacancies in the experiments described in the Experimental section. We found that the calculated Pb vacancy concentration should be about 3.5%, which is within the typical experimental value range (2–8%). Room temperature d^0 ferromagnetism in PbS films can be used in different practical areas such as spintronic based devices, magnetic recording of information in computers, *etc.* There is one feature of PbS d^0 ferromagnetism that makes this material special for fundamental research. PbS ferromagnetism can exhibit topologically driven spatial magnetic moment distributions (*e.g.*, magnetic skyrmions) because of large spin–orbit coupling.

This work was supported by a grant (No. DMR-1710512) from the U.S. National Science Foundation to the University of Wyoming.

Conflicts of interest

There are no conflicts to declare.

References

1 A. H. MacDonald, P. Schiffer and N. Samarth, *Nat. Mater.*, 2005, **4**(3), 1325.
2 T. Dietl and H. Ohno, *Rev. Mod. Phys.*, 2014, **86**(1), 187–251.
3 D. Hoffman, B. Meyer, A. Ekimov, I. Merkulov, A. L. Efros, M. Rosen, G. Couino, T. Gacoin and J. Boilot, *Solid State Commun.*, 2000, **114**(10), 547–550.
4 B. B. Srivastava, S. Jana, N. S. Karan, S. Paria, N. R. Jana, D. Sarma and N. Pradhan, *J. Phys. Chem. Lett.*, 2010, **1**(9), 1454–1458.
5 R. Bhargava, D. Gallagher, X. Hong and A. Nurmikko, *Phys. Rev. Lett.*, 1994, **72**(3), 416.
6 A. Bol and A. Meijerink, *Phys. Rev. B: Condens. Matter Mater. Phys.*, 1998, **58**(24), R15997.
7 J. Suyver, S. Wuister, J. Kelly and A. Meijerink, *Phys. Chem. Chem. Phys.*, 2000, **2**(23), 5445–5448.
8 D. J. Norris, N. Yao, F. T. Charnock and T. A. Kennedy, *Nano Lett.*, 2001, **1**(1), 3–7.
9 D. W. Langer and H. J. Richter, *Phys. Rev.*, 1966, **146**(2), 554.
10 N. Pradhan and X. Peng, *J. Am. Chem. Soc.*, 2007, **129**(11), 3339–3347.
11 M. A. Malik, P. O'Brien and N. Revaprasadu, *J. Mater. Chem.*, 2001, **11**(9), 2382–2386.
12 S. Salimian and S. F. Shayesteh, *J. Supercond. Novel Magn.*, 2012, **25**(6), 2009–2014.
13 V. Proshchenko and Y. Dahnovsky, *J. Phys. Chem. C*, 2014, **118**(48), 28314–28321.
14 V. Proshchenko and Y. Dahnovsky, *Phys. Status Solidi B*, 2015, **252**(10), 2275–2279.
15 A. Pimachev and Y. Dahnovsky, *J. Phys. Chem. C*, 2015, **119**(29), 16941–16946.
16 V. Proshchenko and Y. Dahnovsky, *Photoinduced Processes at Surfaces and in Nanomaterials*, ACS Publications, 2015, pp. 117–135.
17 V. Proshchenko and Y. Dahnovsky, *Phys. Chem. Chem. Phys.*, 2015, **17**(40), 26828–26832.
18 M. Kan, J. Zhou, Q. Sun, Y. Kawazoe and P. Jena, *J. Phys. Lett.*, 2013, **4**(20), 3382–3386.
19 K. Schouteden, T. Ivanova, Z. Li, V. Iancu, E. Janssens and C. Van Haesendonck, *J. Phys. Lett.*, 2015, **6**(6), 1048–1052.
20 A. Saha, A. Shetty, A. Pavan, S. Chattopadhyay, T. Shibata and R. Viswanatha, *J. Phys. Lett.*, 2016, **7**(13), 2420–2428.
21 S. K. Mandal, A. R. Mandal and S. Banerjeet, *ACS Appl. Mater. Interfaces*, 2012, **4**, 205–209.
22 S. S. Farvid, M. Hegde and P. V. Radovanovic, *Chem. Mater.*, 2013, **25**(2), 233–244.
23 N. S. Garnet, V. Ghodsi, L. N. Hutfluss, P. Yin, M. Hegde and P. V. Radovanovic, *J. Phys. Chem. C*, 2017, **121**(3), 1918–1927.
24 A. Walsh, *Appl. Phys. Lett.*, 2011, **98**(26), 261910.
25 T. Dietl, H. Ohno, F. Matsukura, J. Cibert and D. Ferrand, *Science*, 2000, **287**(5455), 1019–1022.
26 M. L. Reed, N. A. El-Masry, H. H. Stadelmaier, M. K. Ritums, M. J. Reed, C. A. Parker, J. C. Roberts and S. M. Bedair, *Appl. Phys. Lett.*, 2001, **79**(21), 3473–3475.
27 P. Sharma, A. Gupta, K. V. Rao, F. J. Owens, R. Sharma, R. Ahuja, J. M. O. Guillen, B. Johansson and G. A. Gehring, *Nat. Mater.*, 2003, **2**(10), 984.
28 P. Dev, Y. Xue and P. Zhang, *Phys. Rev. Lett.*, 2008, **100**(11), 117204.
29 M. Venkatesan, C. Fitzgerald and J. Coey, *Nature*, 2004, **430**(7000), 630.
30 A. Sundaresan, R. Bhargavi, N. Rangarajan, U. Siddesh and C. Rao, *Phys. Rev. B: Condens. Matter Mater. Phys.*, 2006, **74**(16), 161306.
31 N. H. Hong, J. Sakai, N. Poirot and V. Brizé, *Phys. Rev. B: Condens. Matter Mater. Phys.*, 2006, **73**(13), 132404.
32 H. Pan, J. Yi, L. Shen, R. Wu, J. Yang, J. Lin, Y. Feng, J. Ding, L. Van and J. Yin, *Phys. Rev. Lett.*, 2007, **99**(12), 127201.
33 D. Gao, G. Yang, J. Zhang, Z. Zhu, M. Si and D. Xue, *Appl. Phys. Lett.*, 2011, **99**(5), 052502.
34 Z. Zhang, U. Schwingenschlögl and I. S. Roqan, *RSC Adv.*, 2014, **4**(92), 50759–50764.
35 G. Zhu, S. Zhang, Z. Xu, J. Ma and X. Shen, *J. Am. Chem. Soc.*, 2011, **133**(39), 15605–15612.
36 W.-Z. Xiao, L.-l. Wang, Q.-Y. Rong, G. Xiao and B. Meng, *J. Appl. Phys.*, 2014, **115**(21), 213905.
37 V. Proshchenko, A. Karanovich and Y. Dahnovsky, *J. Phys. Chem. C*, 2016, **120**(20), 11253–11261.
38 V. Proshchenko and Y. Dahnovsky, *J. Phys.: Condens. Matter*, 2016, **29**(2), 025803.
39 Z. Li, W. Zhong, X. Li, H. Zeng, G. Wang, W. Wang, Z. Yang and Y. Zhang, *J. Phys. Chem. C*, 2013, **1**(41), 6807–6812.
40 A. Pimachev, V. Proshchenko and Y. Dahnovsky, *J. Phys. Chem. C*, 2017, **121**(35), 19401–19406.

41 A. Pimachev, V. Proshchenko, S. Horoz, O. Sahin and Y. Dahnovsky, *Solid State Commun.*, 2017, **257**, 47–49.
42 M. Khalid, M. Ziese, A. Setzer, P. Esquinazi, M. Lorenz, H. Hochmuth, M. Grundmann, D. Spemann, T. Butz and G. Brauer, *Phys. Rev. B: Condens. Matter Mater. Phys.*, 2009, **80**(3), 035331.
43 B. B. Straumal, A. A. Mazilkin, S. G. Protasova, A. A. Myatiev, P. B. Straumal, G. Schütz, P. A. Van Aken, E. Goering and B. Baretzky, *Phys. Rev. B: Condens. Matter Mater. Phys.*, 2009, **79**(20), 205206.
44 C. Peng, Y. Liang, K. Wang, Y. Zhang, G. Zhao and Y. Wang, *J. Phys. Chem. C*, 2012, **116**(17), 9709–9715.
45 H. Zeng, C. Zhi, Z. Zhang, X. Wei, X. Wang, W. Guo, Y. Bando and D. Golberg, *Nano Lett.*, 2010, **10**(12), 5049–5055.
46 Q. Wang, Q. Sun, G. Chen, Y. Kawazoe and P. Jena, *Phys. Rev. B: Condens. Matter Mater. Phys.*, 2008, **77**(20), 205411.
47 K. E. Knutsen, A. Galeckas, A. Zubiaga, F. Tuomisto, G. C. Farlow, B. G. Svensson and A. Y. Kuznetsov, *Phys. Rev. B: Condens. Matter Mater. Phys.*, 2012, **86**(12), 121203.
48 H. Kaftelen, K. Ocakoglu, R. Thomann, S. Tu, S. Weber and E. Erdem, *Phys. Rev. B: Condens. Matter Mater. Phys.*, 2012, **86**(1), 014113.
49 H. Zeng, X. Xu, Y. Bando, U. K. Gautam, T. Zhai, X. Fang, B. Liu and D. Golberg, *Adv. Funct. Mater.*, 2009, **19**(19), 3165–3172.
50 G. Xing, D. Wang, J. Yi, L. Yang, M. Gao, M. He, J. Yang, J. Ding, T. C. Sum and T. Wu, *Appl. Phys. Lett.*, 2010, **96**(11), 112511.
51 I. Lorite, B. Straube, H. Ohldag, P. Kumar, M. Villafuerte, P. Esquinazi, C. E. Rodriguez Torres, S. Perez de Heluani, V. Antonov and L. Bekenov, *Appl. Phys. Lett.*, 2015, **106**(13), 082406.
52 M. Khalid and P. Esquinazi, *Phys. Rev. B: Condens. Matter Mater. Phys.*, 2012, **85**(13), 134424.
53 P. Esquinazi, W. Hergert, D. Spemann, A. Setzer and A. Ernst, *IEEE Trans. Magn.*, 2013, **49**(8), 4668–4674.
54 R. Viswanatha, D. Naveh, J. R. Chelikowsky, L. Kronik and D. D. Sarma, *J. Phys. Lett.*, 2012, **3**(15), 2009–2014.
55 G. Long, B. Barman, S. Delikanli, Y. Tsung Tsai, P. Zhang, A. Petrou and H. Zeng, *Appl. Phys. Lett.*, 2012, **101**(6), 062410.
56 L. Turyanska, J. Blokland, U. Elfurawi, O. Makarovsky, P. Christianen and A. Patanè, *Phys. Rev. B: Condens. Matter Mater. Phys.*, 2010, **82**(19), 193302.
57 A. Pimachev and Y. Dahnovsky, *J. Phys. Chem. C*, 2015, **119**(29), 16941–16946.
58 G. Rimal, A. K. Pimachev, A. J. Yost, U. Poudyal, S. Maloney, W. Wang, T. Chien, Y. Dahnovsky and J. Tang, *Appl. Phys. Lett.*, 2016, **109**(10), 103901.
59 G. Rimal and J. Tang, *Sci. Rep.*, 2017, **7**, 42224.
60 G. Kresse and J. Furthmüller, *Comput. Mater. Sci.*, 1996, **6**(1), 15–50.
61 G. Kresse and J. Furthmüller, *Phys. Rev. B: Condens. Matter Mater. Phys.*, 1996, **54**(16), 11169–11186.
62 W. Kohn and L. J. Sham, *Phys. Rev.*, 1965, **140**(4A), A1133–A1138.
63 J. Hafner, *J. Comput. Chem.*, 2008, **29**(13), 2044–2078.
64 J. C. Slater, *Phys. Rev.*, 1937, **51**(10), 846–851.
65 D. J. Singh and L. Nordstrom, *Planewaves, Pseudopotentials, and the LAPW Method*, Springer, 2006.
66 M. Weinert, G. Schneider, R. Podloucky and J. Redinger, *J. Phys.: Condens. Matter*, 2009, **21**(8), 084201.
67 P. M. Marcus, *Int. J. Quantum Chem.*, 2009, **1**(S1), 567–588.
68 J. P. Perdew, K. Burke and M. Ernzerhof, *Phys. Rev. Lett.*, 1996, **77**(18), 3865–3868.
69 P. E. Blochl, *Phys. Rev. B: Condens. Matter Mater. Phys.*, 1994, **50**(24), 17953–17979.
70 J. P. Perdew, *Phys. Rev. B: Condens. Matter Mater. Phys.*, 1986, **33**(12), 8822–8824.
71 J. P. Perdew, *AIP Conference Proceedings*, 2001.
72 J. P. Perdew, J. A. Chevary, S. H. Vosko, K. A. Jackson, M. R. Pederson, D. J. Singh and C. Fiolhais, *Phys. Rev. B: Condens. Matter Mater. Phys.*, 1993, **48**(7), 4978.
73 P. E. Blöchl, O. Jepsen and O. K. Andersen, *Phys. Rev. B: Condens. Matter Mater. Phys.*, 1994, **49**(23), 16223–16233.
74 G. Kresse and D. Joubert, *Phys. Rev. B: Condens. Matter Mater. Phys.*, 1999, **59**(3), 1758–1775.
75 C. Li, A. J. Freeman, H. J. F. Jansen and C. L. Fu, *Phys. Rev. B: Condens. Matter Mater. Phys.*, 1990, **42**(9), 5433–5442.
76 D. D. Koelling and B. N. Harmon, *J. Phys. C: Solid State Phys.*, 1977, **10**(16), 3107.
77 S. Christensen, N. Bindzus, M. Sist, M. Takata and B. B. Iversen, *Phys. Chem. Chem. Phys.*, 2016, **18**(23), 15874–15883.

